Pergamon

Int. J. Heat Mass Transfer. Vol. 41, No. 1, pp. 45–59, 1998

Printed in Great Britain
0017-9310/98 $19.00+0.00

PII: S0017-9310(97)00113-0

Forced convection heat transfer from a flat plate: the conjugate problem

M. VYNNYCKY†
Tohoku National Industrial Research Institute, 4-2-1 Nigatake, Miyagino-Ku, Sendai, 983 Japan

S. KIMURA
Department of Mechanical Engineering, Kanazawa University, 2-40-20 Kodatsuno, Kanazawa, 920 Japan

K. KANEV
Visual Science Laboratory, Inc., Awajicho MH bldg, 2-21 Kanda Awajicho, Chiyoda-Ku, Tokyo, 101 Japan

and

I. POP
University of Cluj, Faculty of Mathematics, R-3400 Cluj, CP 253 Romania

(*Received* 29 *November* 1996 *and in final form* 21 *April* 1997)

Abstract—Heat transfer associated with the forced convection flow over a conducting slab sited in an aligned uniform stream is investigated analytically and numerically. Both internal and external thermal conductivities are taken into consideration by means of a conjugate model consisting of the full Navier–Stokes equations for the fluid medium and the energy equations for both the fluid and the slab. The analysis facilitates the investigation of the effects of the Reynolds number (Re), the Prandtl number (Pr), the thermal conductivity ratio (k) between the slab and the fluid medium and the slab aspect ratio (λ) on the heat transfer characteristics. For $Re \gg 1$, boundary-layer theory is used to derive two methods of solution whose results are compared with the full numerical solutions. © 1997 Elsevier Science Ltd.

1. INTRODUCTION

It has become increasingly apparent that conjugate heat transfer regimes occur frequently in practice and that an understanding of them is crucial in many processes. Typical applications where this is true are the entrance regimes of pipe or channel flows [1, 2]. In addition, flows through tunnels or caves that communicate heat with the surrounding rock walls and determine the thermal or environmental conditions also fall in this category; in fact, problems involving insulated or isothermal tunnel walls have been investigated already [3, 4]. Another area of application is in electronic device cooling; due to the low thermal conductivity of molding materials in semiconductor devices, it is critical to design a cooling system that keeps the device temperature below some specified value [5, 6].

The reference work for the coupling of forced convective heat transfer in a boundary-layer flow over a flat plate of finite thickness with two-dimensional thermal conduction in the solid plate is due to Perelman [7]. Apparently, he was the first to present a closed-form expression for the temperature and the local Nusselt number at the fluid–solid interface. Later, Luikov *et al.* [8] obtained an exact solution for the interfacial temperature, reducing the problem, by a generalized Fourier sine transform, to a singular integral equation. The solution is presented in a complicated form and does not easily permit a comparison with the corresponding traditional (non-conjugate) problem. It was again Luikov [9] who gave an approximate solution of this problem assuming that the temperature in the plate varies linearly with the normal distance from its surface, thereby neglecting axial conduction in the plate. However, in both these papers [8, 9], no numerical results were reported. The case of a plate of finite length was analyzed in detail by Sakakibara *et al.* [10] by expanding the fluid–solid interfacial temperature as a power series in the square root of distance along the flat plate, with unknown coefficients to be determined. It was found by these authors that the interfacial temperature is influenced markedly by the wall conduction when the plate is short and/or thick and its thermal conductivity is higher than that of the surrounding fluid.

An extension of the results reported in refs. [8, 9] was

† Present address: Department of Mechanics, Royal Institute of Technology, S-100 44 Stockholm, Sweden.

NOMENCLATURE

A	constant
a	thickness of the conducting slab
b	length of the conducting slab
C_d	drag coefficient
I_n	integrals in equation (103)
k_f	thermal conductivity of the fluid medium
k_s	thermal conductivity of the plate
k	thermal conductivity ratio, k_s/k_f
Nu	dimensionless local Nusselt number
$\bar{N}u$	dimensionless average Nusselt number
T_c	constant temperature of heated side of slab
T_∞	constant temperature of ambient fluid
Pr	Prandtl number for the fluid, ν/α
Q	constant
Re	Reynolds number for the fluid, bU_∞/ν
u, v	dimensional velocity components along (x, y) axes
$\hat{u}, \hat{v}$	dimensionless velocity components along (x, y) axes, $(u, v)/U_\infty$
U_∞	velocity of the ambient fluid
x, y	dimensional Cartesian coordinates along and normal to the plate
$\hat{x}, \hat{y}$	dimensional Cartesian coordinates $(x, y)/b$
x_∞	size of computational domain in x-direction
y_∞	size of computational domain in y-direction.

Greek symbols

α	thermal diffusivity
β	coefficient of thermal expansion
γ	constant
ΔT	temperature difference, $T_c - T_\infty$
$\Delta\theta$	temperature increment
ζ	similarity variable
θ_s	dimensionless temperature in the solid
θ_f	dimensionless temperature in the fluid medium
θ_b	dimensionless boundary temperature
$\bar{\theta}_b$	dimensionless average boundary temperature
θ_0	constant
λ	aspect ratio, a/b
μ	constant
ν	kinematic viscosity
σ	dimensionless constant ($Re^{1/2}/k$ or $(Re\,Pr)^{1/2}/k$)
τ	dimensionless constant ($k/\lambda(Re\,Pr)^{1/2}$)
χ	constant
ψ	dimensionless streamfunction
ω	dimensionless vorticity.

Subscripts

∞	ambient conduction
i, j	nodal quantities.

Superscripts

m	iterative order
$\bar{}$	averaged quantities.

obtained by Payvar [11] for high Prandtl numbers. Karvinen [12, 13] improved the analysis made by Payvar [11] and also presented an iterative technique for solving numerically the problem of conjugate heat transfer for a flat plate in the presence of internal heat sources. A further contribution was made by Chida and Katto [14] who solved the problem by vectorial dimensional analysis. Gosse [15] has given an analytical solution for large values of the distance along the plate far downstream from the leading edge of the plate. Recently Mori *et al.* [16] extended the work by Sakakibara *et al.* [10] by combining mass transfer with the conjugate heat transfer between the flow and the solid plate through the vapour–liquid equilibrium relation. Distributions of interfacial temperature, the local Nusselt and local Sherwood numbers were calculated for a parallel-flow case where the Prandtl and Schmidt number were equal to unity.

The literature on conjugate forced convection heat transfer indicates also some recent papers which follow Luikov's [9] one-dimensional approximation of the conduction process in a flat plate. This model problem has been considered in recent years by several investigators including Pozzi and Lupo [17], Yu *et al.* [18], Pop and Ingham [19] and Pozzi *et al.* [20], among others, for simple practical uses or further theoretical extensions. However, the validity and the applicability of the simplification considered in these papers must be further examined by detailed analysis including also axial thermal conduction in the plate. It is this question which motivates the present work.

In this paper, we solve the two-dimensional conjugate heat transfer problem for a rectangular thermally conducting slab. The governing equations are first developed in dimensionless stream function-vorticity-temperature form and then solved numerically using a finite-difference method for a wide range of different values of the four non-dimensional parameters that are present in the problem: the Reynolds number (Re), the Prandtl number (Pr), the aspect

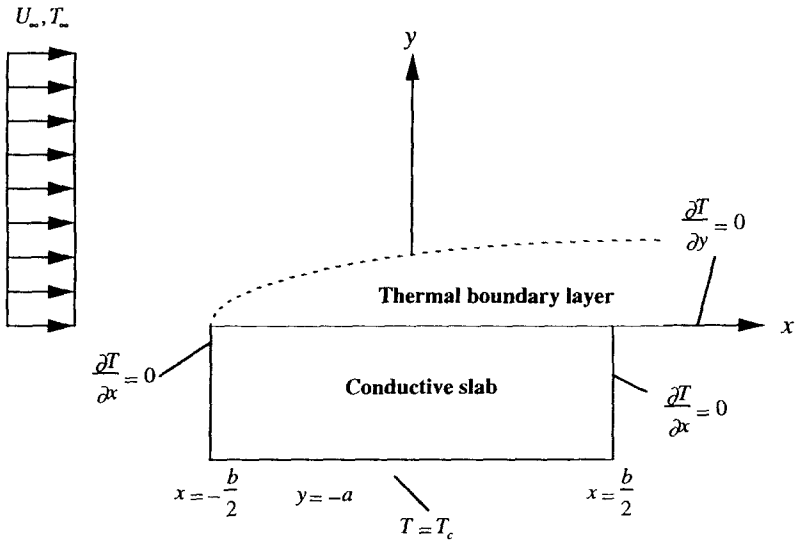

Fig. 1. Physical model and coordinate system.

ratio of the slab (λ) and the thermal conductivity ratio of the slab and the fluid (k). For a thermal and viscous boundary-layer regime, two approaches are presented: one couples conduction in the solid with the boundary-layer flow of the fluid to give a non-linear problem which is solved numerically using the Keller–Box method and relaxation, the other involves the derivation of approximate analytical one-dimensional solutions. The first method encounters numerical difficulties when the value of $Re^{1/2}/k$, for $Pr \gg 1$ [or $(Re\,Pr)^{1/2}/k$, for $Pr \ll 1$] exceeds a critical threshold value which depends on λ. The second method proves to be valid when $k \leqslant 5$ and $Pr \gg 1$.

2. BASIC EQUATIONS

Consider the steady, two-dimensional conjugate heat transfer in a rectangular slab over which a laminar incompressible fluid is flowing. The conducting slab occupies the region $-a \leqslant y \leqslant 0$, $-b/2 \leqslant x \leqslant b/2$, and the ambient forced flow, which occupies $-\infty < x < \infty$, $y \geqslant 0$, has uniform velocity U_∞ and temperature T_∞. A schematic description of the model problem is given in Fig. 1. We assume that the lower side of the slab is held at a uniform temperature $T_c (> T_\infty)$, whilst the sides $x = \mp b/2$ are insulated. It is also assumed that for the fluid region there is no heat flux, no normal outflow and no shear at $y = 0$, $|x| > b/2$. For $y = 0$, $|x| < b/2$, we expect both continuity of temperature and heat flux. Whilst the rationale for most of these boundary conditions is physically evident, that for the conditions at $y = 0$, $|x| > b/2$ is not, and requires a little motivation, as follows.

There is little doubt that the boundary conditions we have assumed are not entirely realistic, particularly at the leading edge ($x = -b/2$). From the fluid-mechanical point of view, it is evident that when a horizontal block is subject to a horizontal uniform flow the horizontal velocity profile at $x = -b/2$ can no longer be uniform, since mass must be conserved at any arbitrary vertical cross-section. At large Reynolds numbers, the situation becomes more complicated because of the possibility of flow separation at the leading edge, subsequent reattachment and the recovery of the laminar boundary layer. From the heat transfer point of view, on the other hand, it is common practice to prescribe a uniform upstream velocity at the leading edge in order to compute the forced convection heat transfer rate over the horizontal surface. Furthermore, this fluid mechanical boundary condition can only be realistic when the plate is extremely thin, or has a downward taper cut at the edge. Therefore, in applying a heat transfer correlation obtained from a Blasius-type velocity profile to a real problem, extreme caution is required.

Nonetheless, we have decided to follow a formulation that is consistent with that employed by previous authors of conjugate heat transfer problems [19]: that is, we prescribe zero shear stress at $y = 0$, which is consistent with a uniform stream boundary condition at $x = -b/2$ for a boundary-layer regime. One advantage in doing so is that we can present and highlight conjugate effects as a deviation from those of an isothermal plate. In addition, once one starts taking into account the full details of incoming flows at the leading edge, it becomes virtually impossible to extract any meaningful compact heat transfer correlation in a simple parametric domain, because the upstream velocity conditions will now depend on both the Reynolds number and the thickness of the upstream slab face. As for the situation downstream of the plate, here too the condition of zero shear stress may appear to be unrealistic, although it may serve

as an adequate approximation to the situation in a grooved channel [6]; of course, for a boundary-layer regime, the boundary condition downstream of the slab should have very little effect on heat transfer at the slab surface itself. The above ideas are expressed mathematically as follows.

Introducing dimensional variables appropriate to the present situation as

$$\hat{x} = \frac{x}{b} \quad \hat{y} = \frac{y}{b} \quad \hat{u} = \frac{u}{U_\infty} \quad \hat{v} = \frac{v}{U_\infty} \quad \hat{\psi} = \frac{\psi}{bU_\infty}$$

$$\hat{\omega} = \frac{b\omega}{U_\infty} \quad \theta_f = \frac{T_f - T_\infty}{\Delta T} \quad \theta_s = \frac{T_s - T_\infty}{\Delta T} \tag{1}$$

where $\Delta T = T_c - T_\infty$ and ψ is the stream function, defined by

$$u = \frac{\partial \psi}{\partial y} \quad v = -\frac{\partial \psi}{\partial x} \tag{2}$$

we drop the hats to obtain the equations governing vorticity and energy transport for the fluid, in the form

$$\nabla^2 \psi = -\omega \tag{3}$$

$$u\frac{\partial \omega}{\partial x} + v\frac{\partial \omega}{\partial y} = \frac{1}{Re}\nabla^2 \omega \tag{4}$$

$$u\frac{\partial \theta_f}{\partial x} + v\frac{\partial \theta_f}{\partial y} = \frac{1}{Re\,Pr}\nabla^2 \theta_f \tag{5}$$

and for the conductive solid slab

$$\nabla^2 \theta_s = 0 \tag{6}$$

where Re and Pr are the Reynolds and Prandtl numbers as given in the Nomenclature, and ∇^2 is the Laplacian in Cartesian coordinates (x, y). The inner boundary conditions for equations (3)–(6) are

$$\psi = \frac{\partial \psi}{\partial y} = 0 \quad \text{on } y = 0 \quad |x| \leqslant \frac{1}{2} \tag{7}$$

$$\psi = \frac{\partial^2 \psi}{\partial y^2} = 0 \quad \text{on } y = 0 \quad |x| > \frac{1}{2} \tag{8}$$

$$\theta_s = \theta_f \quad \text{on } y = 0 \quad |x| \leqslant \frac{1}{2} \tag{9}$$

$$\frac{\partial \theta_f}{\partial y} = k\frac{\partial \theta_s}{\partial y} \quad \text{on } y = 0 \quad |x| \leqslant \frac{1}{2} \tag{10}$$

$$\frac{\partial \theta_f}{\partial y} = 0 \quad \text{on } y = 0 \quad |x| > \frac{1}{2} \tag{11}$$

$$\frac{\partial \theta_s}{\partial x} = 0 \quad \text{on } x = \pm\frac{1}{2} \quad -\lambda \leqslant y \leqslant 0 \tag{12}$$

$$\theta_s = 1 \quad \text{on } y = -\lambda \quad |x| \leqslant \tfrac{1}{2} \tag{13}$$

where $\lambda = a/b$ is the aspect ratio of the conducting slab and $k = k_s/k_f$ is the ratio of the thermal conductivities of the conducting solid and the fluid medium. For the outer boundary conditions, we expect

$$\theta_f \to 0 \quad \text{as } y \to \infty \quad |x| \to \infty \tag{14}$$

$$\frac{\partial \psi}{\partial y} \to 1 \quad \text{as } y \to \infty \quad |x| \to \infty \tag{15}$$

$$\omega \to 0 \quad \text{as } y \to \infty \quad |x| \to \infty \tag{16}$$

although we discuss the implementation of these in greater detail in Section 4. The physical quantities of greatest interest are then the dimensionless local Nusselt number, given by

$$Nu = -\left(\frac{\partial \theta_f}{\partial y}\right)_{y=0} \quad |x| \leqslant \frac{1}{2} \tag{17}$$

and the dimensionless average Nusselt number, defined as

$$\bar{Nu} = \int_{-1/2}^{1/2} Nu\,dx. \tag{18}$$

3. THEORETICAL CONSIDERATIONS FOR $Re \gg 1$

For the case $Re \gg 1$, conductive heat flow in the solid is coupled to the convective heat flow within the thermal and viscous boundary layers that are present at the conjugate boundary. Denoting by θ_0 the temperature at $(-1/2, 0)$, where it is clear that $0 \leqslant \theta_0 \leqslant 1$, a total of four cases emerge, namely $\theta_0 > 0$ and $\theta_0 = 0$ when $Pr \geqslant 1$ and $Pr \ll 1$, and we treat these as follows.

3.1. $Pr \geqslant 1$

For $\theta_0 > 0$, the appropriate rescalings are given by

$$\psi = Re^{-1/2}\Psi \quad \omega = Re^{1/2}\Omega \quad y = Re^{-1/2}Y \tag{19}$$

so that, on invoking the boundary-layer approximation, equations (3)–(5) reduce to

$$\frac{\partial^2 \Psi}{\partial Y^2} = -\Omega \tag{20}$$

$$\frac{\partial \Psi}{\partial Y}\frac{\partial \Omega}{\partial} - \frac{\partial \Psi}{\partial X}\frac{\partial \Omega}{\partial Y} = \frac{\partial^2 \Omega}{\partial Y^2} \tag{21}$$

$$Pr\left(\frac{\partial \Psi}{\partial Y}\frac{\partial \theta_f}{\partial X} - \frac{\partial \Psi}{\partial X}\frac{\partial \theta_f}{\partial Y}\right) = \frac{\partial^2 \theta_f}{\partial Y^2} \tag{22}$$

from equations (20) and (21), we eliminate Ω and integrate once with respect to Y to obtain

$$\frac{\partial \Psi}{\partial Y}\frac{\partial^2 \Psi}{\partial Y \partial X} - \frac{\partial \Psi}{\partial X}\frac{\partial^2 \Psi}{\partial Y^2} = \frac{\partial^3 \Psi}{\partial Y^3} \tag{23}$$

where $X = x + 1/2$, with the start of the boundary layer now at $X = 0$. The boundary conditions relevant to the layer are now

$$\Psi = \frac{\partial \Psi}{\partial Y} = 0 \quad \text{on } Y = 0 \quad X \geqslant 0 \tag{24}$$

$$\theta_f = \theta_s \quad \text{on } Y = 0 \quad 0 \leqslant X \leqslant 1 \tag{25}$$

$$\frac{\partial \theta_f}{\partial Y} = \frac{1}{\sigma}\frac{\partial \theta_s}{\partial y} \quad \text{on } Y = 0 \quad 0 \leqslant X \leqslant 1 \tag{26}$$

$$\frac{\partial \Psi}{\partial Y} \to 1 \quad \theta_f \to 0 \quad \Omega \to 0 \quad \text{as } Y \to \infty \tag{27}$$

where $\sigma = Re^{1/2}/k$ is a dimensionless parameter. Initial conditions are also required at $X = 0$. These come from assuming that there is a uniform stream at ambient temperature for $X \leqslant 0$, so that the appropriate conditions are

$$\frac{\partial \Psi}{\partial Y} = 1 \quad \text{at } X = 0 \tag{28}$$

$$\theta_f = 0 \quad \text{at } X = 0 \tag{29}$$

we return to the validity of these assumptions in Section 5.

For the purpose of analytical development and ultimate numerical solution, it is better to reformulate equations (23)–(29) using similarity-like variables. Writing

$$\Psi(X, Y) = X^{1/2}F(X, \zeta) \quad \theta_f(X, Y) = G(X, \zeta)$$

$$\zeta = \frac{Y}{X^{1/2}} \tag{30}$$

equations (23) and (22) reduce to

$$F''' + \frac{FF''}{2} = X\left(F'\frac{\partial F'}{\partial X} - F''\frac{\partial F}{\partial X}\right) \tag{31}$$

$$\frac{G''}{Pr} + \frac{FG'}{2} = X\left(F'\frac{\partial G}{\partial X} - G'\frac{\partial F}{\partial X}\right) \tag{32}$$

where the primes denote differentiation with respect to ζ. The boundary conditions for $0 \leqslant X \leqslant 1$ in terms of F and G are

$$F = F' = 0 \quad \text{on } \zeta = 0 \tag{33}$$

$$\theta_s = G \quad \text{on } \zeta = 0 \tag{34}$$

$$\frac{\partial \theta_s}{\partial y} = \frac{\sigma}{X^{1/2}}G' \quad \text{on } \zeta = 0 \tag{35}$$

$$F' \to 1 \quad G \to 0 \quad \text{as } \zeta \to \infty \tag{36}$$

with equations (28) and (29) satisfied automatically by the choice of variables. Letting $X \to 0$, we arrive at the ordinary differential equations

$$F''' + \frac{FF''}{2} = 0 \tag{37}$$

$$\frac{G''}{Pr} + \frac{FG'}{2} = 0 \tag{38}$$

subject to

$$F = F' = 0 \quad \text{on } \zeta = 0 \tag{39}$$

$$F' \to 1 \quad G \to 0 \quad \text{as } \zeta \to \infty \tag{40}$$

but with equation (34) now replaced by

$$G = \theta_0 \quad \text{on } \zeta = 0 \tag{41}$$

where the constant θ_0 is, of course, as yet unknown. Furthermore, the canonical substitution $G = \theta_0\hat{G}$, removes θ_0 from the system of equations (37)–(41), which may be solved once and for all ahead of the rest of the computations.

Now, we observe that from the condition for continuity of heat flux at the conjugate boundary in the vicinity of $X = 0$

$$\frac{\partial \theta_s}{\partial y} = \frac{\sigma\theta_0}{X^{1/2}}\hat{G}'(0) \tag{42}$$

so that the heat flux has an integrable singularity, which we remove as follows. Introducing plane polar coordinates (r, ϕ), given by

$$X = r\cos\phi \quad Y = r\sin\phi$$

we note that boundary conditions (12) and (42) become

$$\frac{\partial \theta_s}{\partial \phi} = 0 \quad \text{on } \phi = -\frac{\pi}{2} \tag{43}$$

$$\frac{\partial \theta_s}{\partial \phi} = \sigma\theta_0\hat{G}'(0)r^{1/2} \quad \text{on } \phi = 0. \tag{44}$$

A harmonic function which satisfies these boundary conditions is

$$\hat{\theta}_s(r, \phi) = Ar^{1/2}\sin\frac{\phi}{2} \tag{45}$$

where

$$A = -2\sqrt{2}\sigma\theta_0\hat{G}'(0) \tag{46}$$

so that we may remove the singularity at $r = 0$ by writing $\theta_s = \hat{\theta}_s + \theta_s^*$. Thence, θ_s^* satisfies

$$\nabla^2\theta_s^* = 0 \tag{47}$$

subject to

$$\theta_s^* = \theta_0\hat{G} - \hat{\theta}_s \quad \text{on } y = 0 \quad 0 \leqslant X \leqslant 1 \tag{48}$$

$$\frac{\partial \theta_s^*}{\partial y} = \frac{\sigma\theta_0}{X^{1/2}}\hat{G}' - \frac{\partial \hat{\theta}_s}{\partial y} \quad \text{on } y = 0 \quad 0 \leqslant X \leqslant 1 \tag{49}$$

$$\frac{\partial \theta_s^*}{\partial X} = 0 \quad \text{on } X = 0 \quad -\lambda \leqslant y \leqslant 0 \tag{50}$$

$$\frac{\partial \theta_s^*}{\partial X} = -\frac{\partial \hat{\theta}_s}{\partial y} \quad \text{on } X = 1 \quad -\lambda \leqslant y \leqslant 0 \tag{51}$$

$$\theta_s^* = 1 - \hat{\theta}_s \quad \text{on } y = -\lambda \quad 0 \leqslant X \leqslant 1. \tag{52}$$

Recast into this form, with the singularity at $r = 0$ removed, the equations are amenable to numerical solution by methods to be described shortly, provided

$\theta_0 > 0$. The case when $\theta_0 = 0$ proceeds slightly differently, however, and we include it for completeness.

Here, the similarity-like variables are

$$\Psi(X, Y) = X^{1/2} F(X, \zeta) \quad \theta_f(X, Y) = X^{1/2} G(X, \zeta)$$

$$\zeta = \frac{Y}{X^{1/2}} \tag{53}$$

with governing equations

$$F''' + \frac{FF''}{2} = X\left(F' \frac{\partial F'}{\partial X} F'' - \frac{\partial F}{\partial X}\right) \tag{54}$$

$$\frac{G''}{Pr} + \frac{1}{2}(FG' - GF') = X\left(F' \frac{\partial G}{\partial X} - G' \frac{\partial F}{\partial X}\right) \tag{55}$$

and boundary conditions for $0 \leqslant x \leqslant 1$

$$F = F' = 0 \quad \text{on } \zeta = 0 \tag{56}$$

$$\theta_s = X^{1/2} G \quad \text{on } \zeta = 0 \tag{57}$$

$$\frac{\partial \theta_s}{\partial y} = \frac{\sigma}{X^{1/2}} G' \quad \text{on } \zeta = 0 \tag{58}$$

$$F' \to 1 \quad G \to 0 \quad \text{as } \zeta \to \infty. \tag{59}$$

Letting $X \to 0$, we arrive at

$$F''' + \frac{FF''}{2} = 0 \tag{60}$$

$$\frac{G''}{Pr} + \frac{1}{2}(FG' - GF') = 0 \tag{61}$$

subject to

$$F = F' = 0 \quad \text{on } \zeta = 0 \tag{62}$$

$$F' \to 1 \quad G \to 0 \quad \text{as } \zeta \to \infty \tag{63}$$

with the initial conditions already satisfied thanks to the choice of variables. Here, the apparent shortfall in boundary conditions is made up for by observing that the canonical forms $G = Q\hat{G}$ are also solutions to equations (60)–(63), with Q a constant to be determined. Subsequently, $\hat{F}$ and $\hat{G}$ satisfy equations (60)–(63), with the extra boundary condition appearing in the form

$$\hat{G}'(0) = -1 \tag{64}$$

and with Q being determined from the continuity of heat flux at $Y = 0$ once the solution for θ_s has been found. This time, there is no singularity near the origin with respect to θ_s, which now satisfies the boundary conditions

$$\theta_s = QX^{1/2}\hat{G} \quad \text{on } y = 0 \quad 0 < X < 1 \tag{65}$$

$$\frac{\partial \theta_s}{\partial y} = Q\sigma \hat{G}' \quad \text{on } y = 0 \quad 0 < X < 1 \tag{66}$$

$$\theta_s = 1 \quad \text{on } y = -\lambda \quad 0 < X < 1 \tag{67}$$

$$\frac{\partial \theta_s}{\partial x} = 0 \quad \text{on } X = 0, 1 \quad -\lambda \leqslant y \leqslant 0. \tag{68}$$

Although we have not used this formulation for our numerical scheme, we note here that it is the appropriate one to choose in the thin-slab limit ($\lambda \to 0$) considered previously by Pop and Ingham [19].

3.2. $Pr \ll 1$

For this regime, the thermal boundary layer, of thickness $(Re\,Pr)^{-1/2}$, is much thicker than the viscous. To obtain the governing equations for θ_f, which replace equations (23)–(29), we refer back to the scalings given by equation (19), except this time with

$$y = (Re\,Pr)^{-1/2} Y.$$

At leading order, the boundary-layer equations are now

$$\frac{\partial \Psi}{\partial Y}\frac{\partial^2 \Psi}{\partial Y \partial X} - \frac{\partial \Psi}{\partial X}\frac{\partial^2 \Psi}{\partial Y^2} = 0 \tag{69}$$

$$\frac{\partial \Psi}{\partial Y}\frac{\partial \theta_f}{\partial X} - \frac{\partial \Psi}{\partial X}\frac{\partial \theta_f}{\partial Y} = \frac{\partial^2 \theta_f}{\partial Y^2} \tag{70}$$

from these, we can obtain

$$\Psi \equiv Y \tag{71}$$

$$\frac{\partial \theta_f}{\partial X} = \frac{\partial^2 \theta_f}{\partial Y^2} \tag{72}$$

where equation (72) satisfies the boundary conditions

$$\theta_f = \theta_s \quad \text{on } Y = 0 \quad 0 \leqslant X \leqslant 1 \tag{73}$$

$$\frac{\partial \theta_f}{\partial Y} = \frac{1}{\sigma}\frac{\partial \theta_s}{\partial y} \quad \text{on } Y = 0 \quad 0 \leqslant X \leqslant 1 \tag{74}$$

$$\theta_f \to 0 \quad \text{as } Y \to \infty \tag{75}$$

$$\theta_f = 0 \quad \text{at } X = 0 \tag{76}$$

and where σ is now given by $\sigma = (Re\,Pr)^{1/2}/k$. The equations for the viscous boundary layer of thickness $Re^{-1/2}$, incidentally, remain the same as before, but their solution is not necessary for determining θ_f.

Treating once again the case when $\theta_0 > 0$ first, we note a discontinuity in the boundary conditions for θ_f at $X = 0$, $Y = 0$ which is liable to cause numerical difficulties. The singularity may be removed using a coordinate transformation, as follows. Writing

$$\eta = \frac{Y}{X^{1/2}} \quad S = X^{1/2} \tag{77}$$

equation (72) becomes

$$\frac{\partial^2 \theta_f}{\partial \eta^2} = \frac{1}{2}\left(S\frac{\partial \theta_f}{\partial S} - \eta \frac{\partial \theta_f}{\partial \eta}\right) \tag{78}$$

subject to

$$\theta_s = \theta_f \quad \text{on } \eta = 0 \quad 0 \leqslant S \leqslant 1 \tag{79}$$

$$\frac{1}{S}\frac{\partial \theta_f}{\partial \eta} = \frac{1}{\sigma}\frac{\partial \theta_s}{\partial y} \quad \text{on } \eta = 0 \quad 0 \leqslant S \leqslant 1 \tag{80}$$

$$\theta_f \to 0 \quad \text{as } \eta \to \infty. \tag{81}$$

Furthermore, equation (76) is replaced by considering the limit of equations (78)–(81) as $S \to 0$; in particular, we obtain the ordinary differential equation

$$\frac{d^2\theta_f}{d\eta^2} + \frac{\eta}{2}\frac{d\theta_f}{d\eta} = 0 \tag{82}$$

subject to

$$\theta_f \to 0 \quad \text{as } \eta \to \infty \tag{83}$$

$$\theta_f = 0 \quad \text{on } \eta = 0 \tag{84}$$

which leads to the solution

$$\theta_f(\eta, 0) = \theta_0 \operatorname{erfc}\left(\frac{\eta}{2}\right) \tag{85}$$

where $\operatorname{erfc}(X)$ denotes the complementary error function given by

$$\operatorname{erfc}(X) = \frac{2}{\pi^{1/2}} \int_X^\infty e^{-s^2}\, ds.$$

Subsequently, we arrive at

$$\frac{\partial\theta_s}{\partial y} \sim \frac{\sigma\theta_0}{(\pi X)^{1/2}} \quad \text{on } y = 0 \quad \text{as } X \to 0$$

which suggests, by analogy with equations (42) and (46), that we should take

$$A = \frac{2\sqrt{2}\sigma\theta_0}{\pi^{1/2}} \tag{86}$$

in order to remove the singularity in θ_s. As a corollary to the above considerations, we note finally that when $\theta_0 = 0$, there is no singularity at $X = 0$, $Y = 0$, and the equations can be solved numerically without recourse to transformation equation (77).

Finally, we observe that in the thin-slab limit considered by Pop and Ingham [19], a closed-form solution may be derived for $Pr \ll 1$, as follows. In this situation we have that

$$\frac{\partial^2\theta_s}{\partial y^2} = 0 \tag{87}$$

which then gives

$$\theta_s(X, y) = \frac{(\theta_b(X) - 1)}{\lambda} y + \theta_b(X) \tag{88}$$

which leads to equation (72), subject to equations (75) and (76) and

$$\frac{\partial\theta_f}{\partial Y} = \tau(\theta_f - 1) \tag{89}$$

where $\tau = k/\lambda(Re\, Pr)^{1/2}$. With reference to Carslaw and Jaeger [21, p. 74], the solution for θ_f for $0 \leqslant X \leqslant 1$ may be written down as

$$\theta_f(X, Y) = \operatorname{erfc}\left(\frac{Y}{2X^{1/2}}\right) - e^{\tau(Y+\tau X)} \operatorname{erfc}\left(\frac{Y}{2X^{1/2}} + \tau X^{1/2}\right) \tag{90}$$

which then gives

$$\theta_b(X) = 1 - e^{\tau^2 X} \operatorname{erfc}(\tau X^{1/2}). \tag{91}$$

3.3. *Solution*

The numerical solution procedure was identical to that used by Vynnycky and Kimura [22], the only difference being the actual form of the boundary-layer equations. In summary, the latter were discretized and solved using the Keller–Box method, as described by Cebeci and Bradshaw [23], whilst regular five-point differencing was used for the slab temperature, with the two temperature distributions being coupled via the conditions at the conjugate boundary which then had to be iterated for; the convergence criterion used was

$$\max_{i,j} |\theta_s^{(m+1)} - \theta_s^{(m)}| < 10^{-7}$$

where m denotes the iteration order, and i and j are indices over y and x, respectively. For those parameter combinations which yielded converged solutions, convergence was obtained within 20 iterations, requiring less than a minute of CPU time on a Cray Supercomputer. However, in common with the results in ref. [22], it became quickly evident that convergence was only possible for sufficiently small values of the parameter σ. For instance, for $Pr = 10^2$ no solutions at all were obtained for $\lambda = 0.25$ and 1, $Re = 500, 10^4$, $k = 1, 2, 5, 20$; for $Pr = 10^{-2}$, further runs carried out in addition to the above indicated that the scheme became non-convergent for, approximately, $\sigma > \sqrt{5}/3$, when $\lambda = 0.25$, and for $\sigma > \sqrt{5}/6$, when $\lambda = 1$.

3.4. *Quasi-two-dimensional analogue*

A simpler approach for determining the temperature profile approximately in the solid when $Re \gg 1$ proves to be valid for certain parameter ranges, to be ascertained in Section 5, or Pr, k and λ. This involves assuming one-dimensional heat flow in the slab in order to obtain a horizontally-averaged Nusselt number and conjugate boundary temperature, which are then used as input for the boundary conditions for a Dirichlet problem for the slab, as follows. We assume first that $Pr \geqslant O(1)$.

Defining the average conjugate boundary temperature $\bar{\theta}_b$ by

$$\bar{\theta}_b = \int_0^1 \theta_f(0, y)\, dX$$

then, on using the scalings of equation (19) and the canonical transformation used after equation (41),

albeit with $\bar{\theta}_b$ replacing θ_0, averaging over $0 \leqslant X \leqslant 1$ gives, for θ_s,

$$\theta_s(y) = \frac{\bar{\theta}_b - 1}{\lambda} y + \bar{\theta}_b. \tag{92}$$

Integrating equation (35) over $0 \leqslant X \leqslant 1$ gives [22]

$$\frac{k}{\lambda}(\bar{\theta}_b - 1) = 2\, Re^{1/2} \bar{\theta}_b \hat{G}'(0) \tag{93}$$

where $\hat{G}'(0)$, which depends only on the Prandtl number, comes from the solution of equations (37)–(41); in fact, a useful correlation, due to Pohlhausen [24], is

$$\hat{G}'(0) = 0.332 Pr^{1/3}. \tag{94}$$

Rearranging (93), we arrive at

$$\bar{\theta}_b(\mu) = \frac{1}{1+\mu} \tag{95}$$

$$\bar{Nu}(\mu, k/\lambda) = \frac{(k/\lambda)\mu}{1+\mu} \tag{96}$$

where

$$\mu = \frac{\lambda\, Pr^{1/3}\, Re^{1/2}}{1.506k}. \tag{97}$$

The case for $Pr \ll 1$, $Re\, Pr \gg 1$ proceeds similarly, except that the equivalent of (93) here is

$$\frac{k}{\lambda}(\bar{\theta}_b - 1) = -\frac{2}{\pi^{1/2}} (Re\, Pr)^{1/2} \bar{\theta}_b \tag{98}$$

and $\bar{\theta}_b$ and $\bar{Nu}$ are once again given by (95) and (96), respectively, except with (97) replaced by

$$\mu = \frac{2\lambda (Re\, Pr)^{1/2}}{k\pi^{1/2}}. \tag{99}$$

With $\bar{\theta}_b$ determined, we proceed with a substitution for $\theta_b(x)$ in the form

$$\theta_b(x) = \chi(x + \tfrac{1}{2})^\gamma \quad -\tfrac{1}{2} \leqslant x \leqslant \tfrac{1}{2} \tag{100}$$

where χ and γ are real constants to be determined as follows. Equation (100), with $\gamma = 1/2$, in fact expresses the actual boundary temperature profile for a non-conjugate problem in which the heated boundary is subjected to a constant flux χ; in the present treatment, however, it is proposed to determine χ based on heat transfer between the solid and the fluid. We continue to work with the parameter γ, incidentally, because analogous results are relevant in a variety of other conjugate problems: for instance, in conjugate free convection past a vertical plate in a Newtonian fluid [22], $\gamma = 1/5$, whereas for the corresponding situation in a porous medium $\gamma = 1/3$ [25]. In particular, χ is given by

$$\chi \int_{-1/2}^{1/2} \left(x + \frac{1}{2}\right)^\gamma \mathrm{d}x = \bar{\theta}_b \tag{101}$$

whence the resulting Dirichlet problem for θ_s, that is equation (6), subject to equations(12) and (13) and

$$\theta_s = \theta_b(x) \quad \text{on } y = 0 \quad -\tfrac{1}{2} \leqslant x \leqslant \tfrac{1}{2} \tag{102}$$

gives a series solution in the form

$$\theta_s(x, y) = -\frac{y}{\lambda} + 2(\gamma+1)\bar{\theta}_b \times \sum_{n=1}^{\infty} I_n \frac{\sinh n\pi(y+\lambda)}{\sinh n\pi\lambda} \cos n\pi \left(z + \frac{1}{2}\right) \tag{103}$$

where the integrals I_n are given by

$$I_n = \int_0^1 x^\gamma \cos n\pi x \, \mathrm{d}x \tag{104}$$

the heat flux at the conjugate boundary is then

$$\left(\frac{\partial \theta_s}{\partial y}\right)_{y=0} = -\frac{1}{\lambda} + 2\bar{\theta}_b(\gamma+1)\pi \times \sum_{n=1}^{\infty} I_n \coth n\pi\lambda \cos n\pi \left(x + \frac{1}{2}\right). \tag{105}$$

4. NUMERICAL SOLUTION

Equations (3)–(6), subject to equations (7)–(16), were solved numerically using a non-uniform Cartesian grid, with the control volume method of Patankar [26] being used to discretize equations (4) and (5), and regular five-point differencing being used for equations (3) and (6). Subsequently, equations (3) and (4) were swept over simultaneously and solved using Gauss–Seidel iteration, subject to a convergence criterion

$$\max_{i,j}(|\psi_{i,j}^{(m)} - \psi_{i,j}^{(m-1)}| \quad |\omega_{i,j}^{(m)} - \omega_{i,j}^{(m-1)}|) < 10^{-8}$$

the velocity field so generated for a particular value of Re was then used as input for equations (5) and (6), which were solved for in the same way. In general, a relaxation parameter of 1.8 was used for equations (3) and (6), and 0.7 for equations (4) and (5), and each calculation required of the order of a few minutes on a Cray Supercomputer.

To deal with the boundary conditions at infinity, we implemented analytical formulae for ψ, ω and θ which we derived in similar fashion to those of Robertson *et al.* [27] for a related problem. Whilst we omit the details of the derivation, we note that the expressions for ψ and ω are exactly the same, although the expression for θ differs slightly, since the boundary conditions for $x > 1/2$ are for zero flux, rather than zero temperature; thence, denoting by x_∞ and y_∞ the finite x- and y-values taken for 'effective' infinity, we quote the necessary results as, for $x = -x_\infty$, $0 \leqslant y \leqslant y_\infty$ and $y = y_\infty$, $-x_\infty \leqslant x \leqslant 0$

$$\theta_f = 0$$

$$\psi \sim y + \frac{C_d}{2}\left[-1 + \frac{1}{\pi}\tan^{-1}\left(\frac{y}{x}\right)\right]$$

$$\omega = 0$$

and for $x = x_\infty$, $0 \leqslant y \leqslant y_\infty$ and $y = y_\infty$, $0 \leqslant x \leqslant x_\infty$

$$\theta_f \sim A x^{-1/2} e^{-RePry^2/4x} + o(r^{-1/2})$$

$$\psi \sim y + \frac{C_d}{2\pi}\tan^{-1}\left(\frac{y}{x}\right) - \frac{C_d}{2}\mathrm{erf}\left(\frac{Re^{1/2}y}{2x^{1/2}}\right) + o(1)$$

$$\omega \sim -\frac{Re^{3/2}C_d}{4\pi^{1/2}}\frac{y}{x^{3/2}}e^{-Rey^2/4x} + o(r^{-1/2})$$

where

$$\mathrm{erf}(X) = 1 - \mathrm{erfc}(X)$$

C_d is the corresponding drag coefficient, given by

$$C_d = -\frac{2}{Re}\int_{-1/2}^{1/2} \omega(x, 0)\,dx$$

and the constant A, given by

$$A = -\frac{1}{(\pi\, Re\, Pr)^{1/2}}\int_{-1/2}^{1/2} \frac{\partial\theta_f}{\partial y}(x, 0)\,dx$$

is derived by considering the balance between the heat lost at the slab surface, and that transported downstream.

We envisaged obtaining results for the range $10^2 \leqslant Re \leqslant 10^4$, $Pr = 10^{-2}$, 10^2 and so a variety of meshes were initially experimented with in order to resolve adequately the thermal and viscous boundary layers present in the fluid; a uniform mesh was always used for the solid. For all computations, a mesh which was uniform in x for the extent of the slab, and whose spacing in x increased geometrically for $1/2 < |x| \leqslant x_\infty$, was used. The spacing in y was also non-uniform and determined geometrically in such a way that there were always 10 points within a distance equal to the magnitude of the shortest physically relevant fluid length scale; thus, for a given Re, in view of the fact that the largest value of Pr used was 10^2, the appropriate distance was $(100Re)^{-1/2}$. For all runs, $x_\infty = y_\infty = 5$ proved to be large enough. Typically, 20 mesh points were used for the y-direction in the fluid, 75 each for the regions upstream and downstream of the plate in the x-direction, and 50×50 points for the slab itself.

For the non-conjugate problem, the method was checked against results available in the literature. Our tests are summarized in Table 1, which compares the results obtained against theoretical results for the scaled drag coefficient and the scaled Nusselt number which pertain in the limit of high Re. The agreement is particularly good in the second and fifth columns, whilst we suspect that a lower value of Pr would need to be taken in order to obtain better agreement towards the bottom of the third column. This view is reinforced by the fact that $\bar{N}u/(Re\,Pr)^{1/2}$ for $Re = 10^4$ increases monotonically as $Pr \to 0$: for instance, we obtained from further computations that for $Pr = 5 \times 10^{-3}$ and $Re\,Pr = 50$, $\bar{N}u/(Re\,Pr)^{1/2} = 1.139$, whilst for $Pr = 10^{-3}$ and $Re\,Pr = 10$, $\bar{N}u/(Re\,Pr)^{1/2} = 1.156$, much more in line with the theoretical value of 1.128. There is a discrepancy of a few percent towards the bottom of the fourth column for $Pr = 1$, probably due to the fact that Nu is integrably singular at $x = \pm 1/2$; this order of error is not uncommon in computations of this sort [22].

5. RESULTS

For the range in Re and Pr mentioned above, numerical results were obtained for $k = 1, 2, 5, 20$, $\lambda = 0.25, 1$. To facilitate understanding, we point out in advance that for Figs. 4–11, we have adopted the convention that full or broken lines are for solutions obtained from Navier–Stokes computations and that shaded and open symbols are for solutions due to the analytical methods of Sections 3.2 and 3.4, respectively; for Figs. 12 and 13, the convention for lines and open symbols is reversed.

First, in Figs. 2 and 3, the isotherm dependency on the various parameters is demonstrated when $Re = 10^4$, $\lambda = 0.25$. In Fig. 2, where $Pr = 10^{-2}$, the lower value of k (a) ensures a far greater temperature drop across the solid than is the case for the higher value (b); also outstanding in (b) is a kink in the isotherm for $\theta = 0.9$ at the conjugate boundary, which is due to the high conductivity ratio between the two media. Figure 3 for the high Prandtl number regime, on the other hand, illustrates that most of the tem-

Table 1. Comparison of scaled C_d and $\bar{N}u$ values for computed solutions with analytical results for $Pr = 10^{-2}$, 1, 10^2

Re	$C_d Re^{1/2}$	$\bar{N}u/(Re\,Pr)^{1/2}$ ($Pr = 10^{-2}$)	$\bar{N}u/Re^{1/2}$ ($Pr = 1$)	$\bar{N}u/Re^{1/2}\,Pr^{1/3}$ ($Pr = 10^2$)
100	1.662	1.215	0.676	0.707
500	1.482	1.035	0.651	0.687
1000	1.431	1.006	0.644	0.682
5000	1.359	0.977	0.634	0.673
10000	1.329	0.972	0.631	0.671
Theoretical	1.328	1.128	0.664	0.664

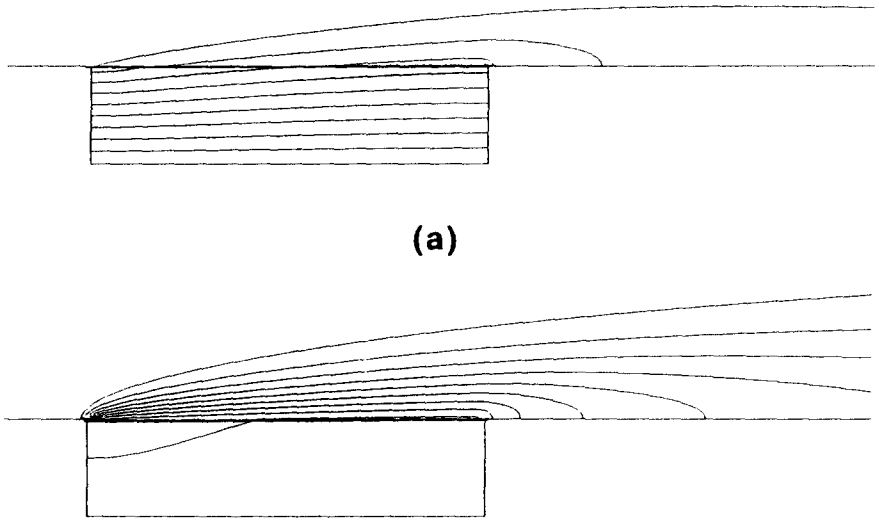

Fig. 2. Isotherms for $Re = 10^4$, $Pr = 10^{-2}$, $\lambda = 0.25$ ($\Delta\theta = 0.1$): (a) $k = 1$; (b) $k = 20$.

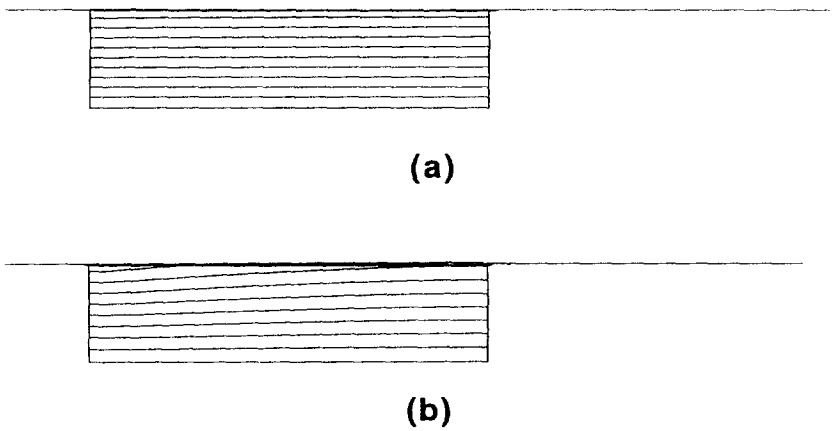

Fig. 3. Isotherms for $Re = 10^4$, $Pr = 10^2$, $\lambda = 0.25$ ($\Delta\theta = 0.1$): (a) $k = 1$; (b) $k = 20$.

perature drop occurs across the solid both for $k = 1$ and 20 and that, in particular in plot (b), any drop that does occur within the fluid is contained within a thin boundary layer adjacent to the surface of the slab.

Figures 4–7 show the local Nusselt number for a range of k values lying between, and including, those used for Figs. 2 and 3, for $\lambda = 0.25$, 1, $Re = 5 \times 10^2$, 10^4. Also included here is a comparison, where possible, with the semi-analytical method of Sections 3.1 and 3.2; however, for the ranges of Re and k that were chosen, the number of converged solutions that were actually obtained is relatively small, since in most cases σ exceeds the threshold values indicated in Section 3.3. The common feature of the Navier–Stokes computations in many of the plots is that of high local Nusselt number at the left-hand end of the conjugate boundary which decreases monotonically for most of the length, before increasing markedly towards the end of the slab; the curves for the analytical solutions do not, unsurprisingly, show this last feature, since no attempt was made to account for the discontinuity in boundary conditions at the slab surface at $(1/2, 0)$ which is responsible for the increase in local Nusselt number. The agreement between the two methods is quite good, given that, as mentioned in Section 4, $Pr = 10^{-2}$ is insufficiently low for good agreement in the limit as $Pr \to 0$. A further observation here is that, particularly in Figs. 6 and 7, the local Nusselt number is approximately constant for most of the conjugate boundary, suggesting that the constant-flux approximation developed in Section 3.4 may provide adequate results for $Pr \gg 1$, provided $k \leqslant 5$; this point is explored further presently.

Figures 8–11 show the conjugate boundary tem-

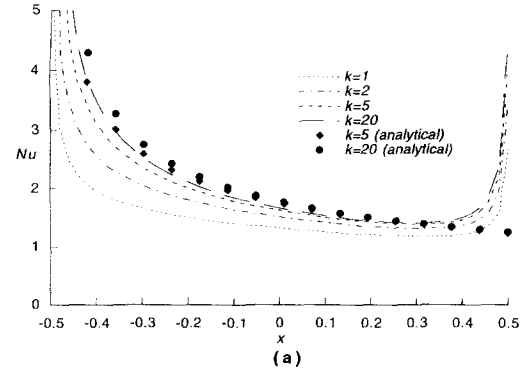

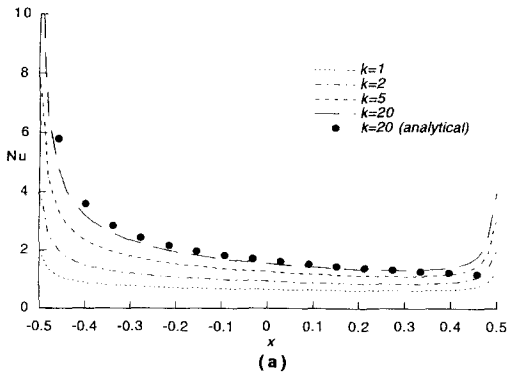

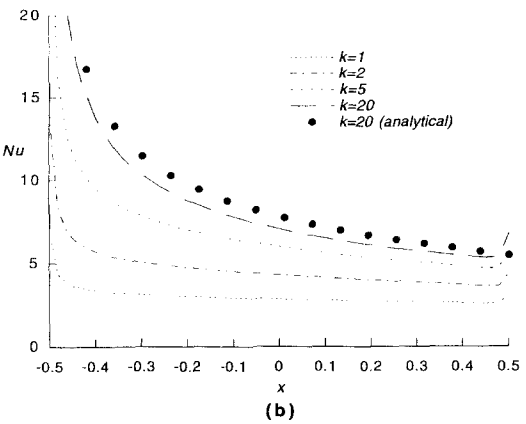

Fig. 4. Local Nusselt number (Nu) vs x for $Pr = 10^{-2}$, $\lambda = 0.25$: (a) $Re = 5 \times 10^2$; (b) $Re = 10^4$.

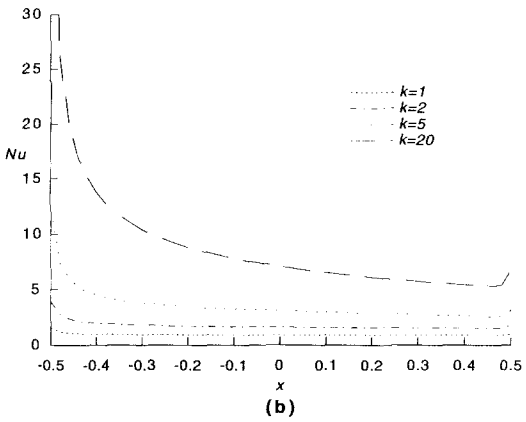

Fig. 5. Local Nusselt number (Nu) vs x for $Pr = 10^{-2}$, $\lambda = 1$: (a) $Re = 5 \times 10^2$; (b) $Re = 10^4$.

perature (θ_b) for Figs. 4–7 respectively; in Figs. 8 and 9, the analytical solution that is referred to is that developed in Section 3.2, while for Figs. 10 and 11 it is that given by (100) under the constant-flux approximation. In Figs. 8 and 9, we see quite good agreement for θ_b, although as in ref. [22], there is a significant difference between the profiles near the leading edge of the slab. A similar point has been discussed before [22], and concerns the assumptions used in employing the boundary conditions (28) and (29) for the start of the boundary layer. By analogy with the earlier paper, one would expect agreement for θ_0 to improve as $Re\,Pr$ is increased, something which plainly does not happen if we compare the results for $k = 20$ in Fig. 8(a, b). Although we have not resolved this issue by computation, it may be suspected that once again the value for Pr is not actually sufficiently low to permit a fair comparison. A further issue of interest is that the numerical method of Section 3.3, both here and in ref. [22], consistently fails where $\theta_0 \leqslant 0.5$, a point worthy of further investigation.

Turning to Figs. 10 and 11, on the other hand, comparison of θ_b does indeed indicate that the constant-flux approximation provides an adequate description of flow within the solid when $Pr \gg 1$, $k \leqslant 5$, since agreement in θ_b subsequently ensures agreement for θ_s by the uniqueness property of the Dirichlet problem. As in earlier conjugate convection studies [22, 25], it is evident from these figures that an increase in the parameter controlling heat flow in the boundary-layer, here $Re\,Pr$, or an increase in λ decreases the boundary temperature, whilst an increase in k increases it.

Figures 12 and 13 summarize the bulk of the computations in terms of the average Nusselt number dependency on Re, as well as comparing these results with the predictions of the analytical formulae (95) and (96). In Fig. 12, we see good agreement for both aspect ratios for $k \leqslant 5$, but note quite substantial deterioration for $k = 20$; the latter feature is once again hardly surprising, since the regime $k \gg 1$ corresponds to an isothermal plate, the solutions to which were discussed in Section 4. In Fig. 13, the results for $Pr = 10^2$ agree well for all four values of k displayed, with agreement for the high k values guaranteed by the results for the isothermal plate shown earlier in Table 1.

In summary, therefore, we obtain agreement to

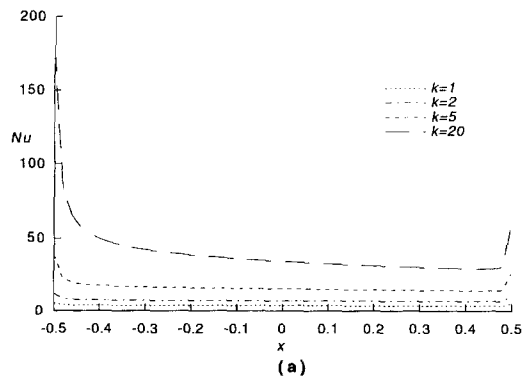

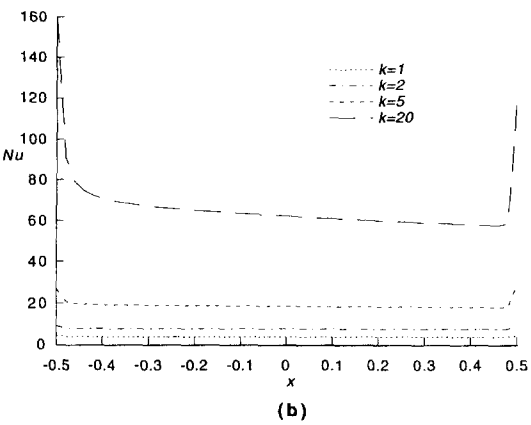

Fig. 6. Local Nusselt number (Nu) vs x for $Pr = 10^2$, $\lambda = 0.25$: (a) $Re = 5 \times 10^2$; (b) $Re = 10^4$.

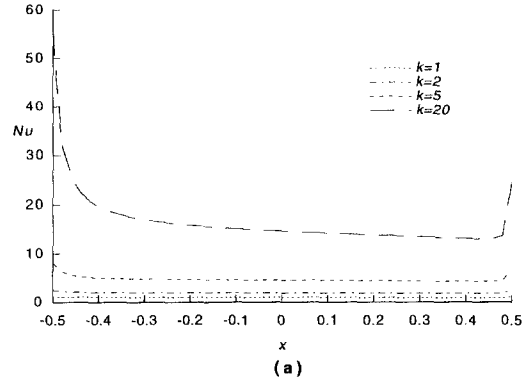

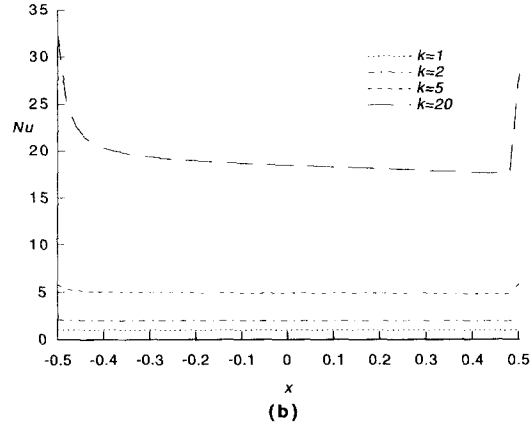

Fig. 7. Local Nusselt number (Nu) vs x for $Pr = 10^2$, $\lambda = 1$: (a) $Re = 5 \times 10^2$; (b) $Re = 10^4$.

within 1 or 2% for $\bar{N}u$, in particular for lower values of k, and agreement to within perhaps 5% when k is as high as 20. As for local quantities θ_b and Nu, quantitative comparison with the coupled conduction-boundary-layer method of Sections 3.1 and 3.2 is only possible for $k \geqslant 5$ and leads to agreement to within a couple of per cent for the majority of the conjugate interface. The leading and trailing edges of the plate tend to be more problematical, with differences in θ_b and Nu sometimes greater than 10%; this is not surprising at the trailing edge, since the asymptotic method, which treats essentially a parabolic system of equations, is not able to capture the temperature drop that occurs in the full elliptic system.

6. CONCLUSIONS

This paper has attempted to provide a comprehensive account of two-dimensional forced convection flow over a slab of both finite length and thickness. The governing momentum and heat transfer equations were solved numerically using an efficient finite-difference scheme for a wide range of the four non-dimensional parameters (Re, Pr, k, λ) that appear in the problem. In addition, the $Re \gg 1$ regime was investigated further using two analytical methods of varying complexity. An averaging method that was developed provides good agreement with the full equations for $k \leqslant 5$ and $Pr \gg 1$, as well as providing good predictions for the mean Nusselt number ($\bar{N}u$) and conjugate boundary temperature ($\bar{\theta}_b$); in particular, the method indicates that $\bar{\theta}_b$ can be reduced, via equation (95), to a function of just one parameter, whilst $\bar{N}u$ reduces to a function of two. A second method which coupled two-dimensional conduction in the slab with convective flow in the adjacent boundary layer was also developed. For $Pr \geqslant 1$, the relevant parameter set is $(Re^{1/2}/k, Pr, \lambda)$, whilst for $Pr \ll 1$, heat flow depends on just $((Re\,Pr)^{1/2}/k, \lambda)$; the greatest simplification, however, comes for $Pr, \lambda \ll 1$, in which case the only governing parameter is $\lambda(Re\,Pr)^{1/2}/k$. Whilst this second method appears able to provide an adequate representation of the heat flow for $Re \gg 1$, its range of applicability was found to be limited owing to convergence difficulties associated with the iterative solution of the discretized equations, particularly for $Pr \gg 1$.

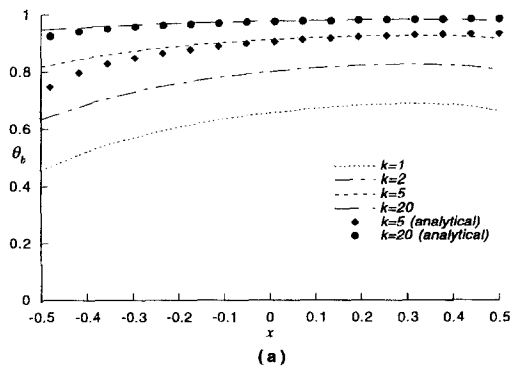

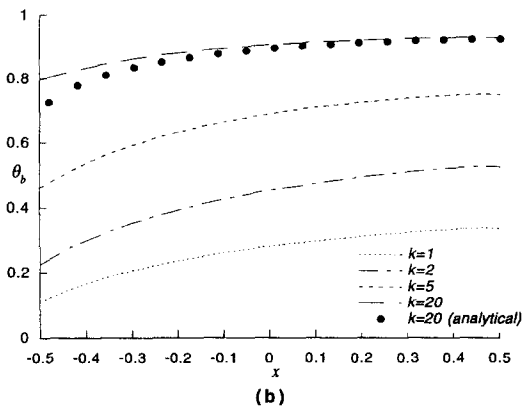

Fig. 8. Conjugate boundary temperature (θ_b) vs x for $Pr = 10^{-2}$, $\lambda = 0.25$: (a) $Re = 5 \times 10^2$; (b) $Re = 10^4$.

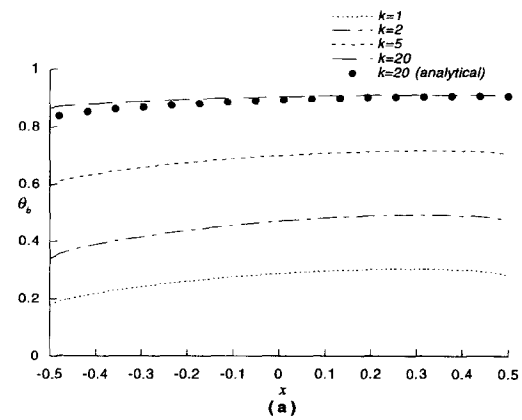

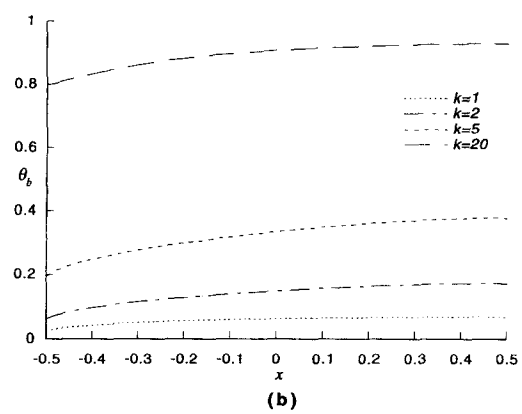

Fig. 9. Conjugate boundary temperature (θ_b) vs x for $Pr = 10^{-2}$, $\lambda = 1$: (a) $Re = 5 \times 10^2$; (b) $Re = 10^4$.

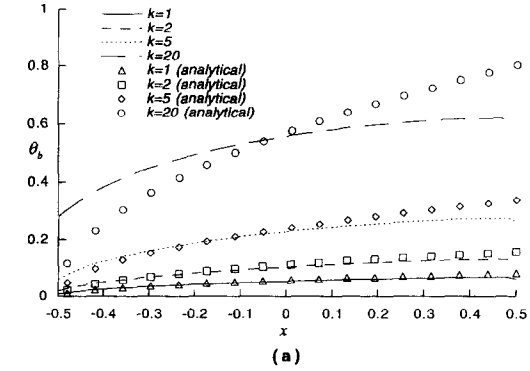

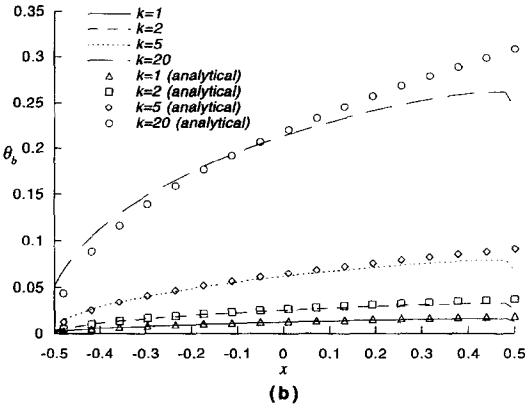

Fig. 10. Conjugate boundary temperature (θ_b) vs x for $Pr = 10^2$, $\lambda = 0.25$: (a) $Re = 5 \times 10^2$; (b) $Re = 10^4$.

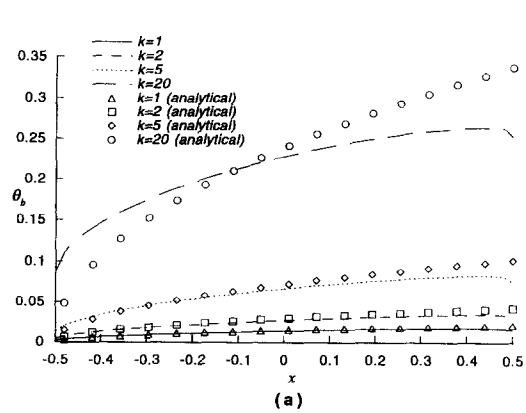

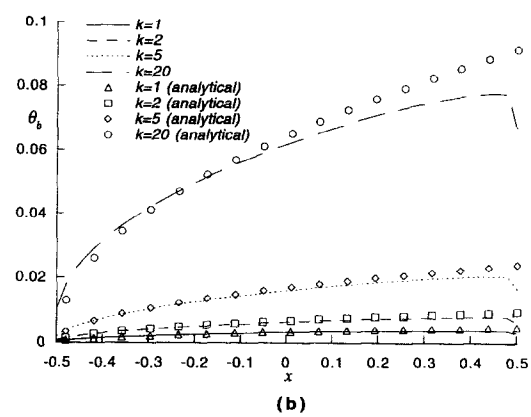

Fig. 11. Conjugate boundary temperature (θ_b) vs x for $Pr = 10^2$, $\lambda = 1$: (a) $Re = 5 \times 10^2$; (b) $Re = 10^4$.

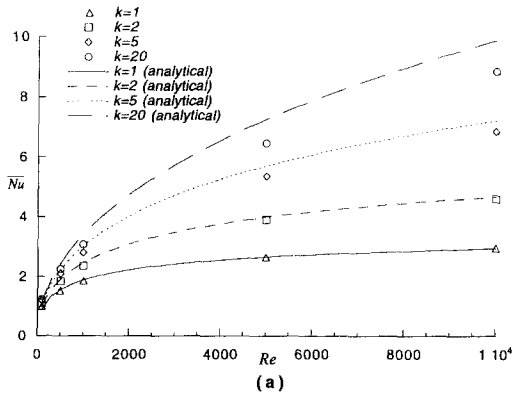

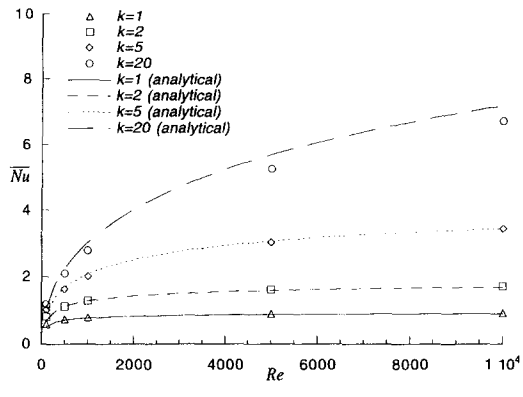

Fig. 12. Average Nusselt number ($\bar{N}u$) vs Re for $Pr = 10^{-2}$: (a) $\lambda = 0.25$; (b) $\lambda = 1$.

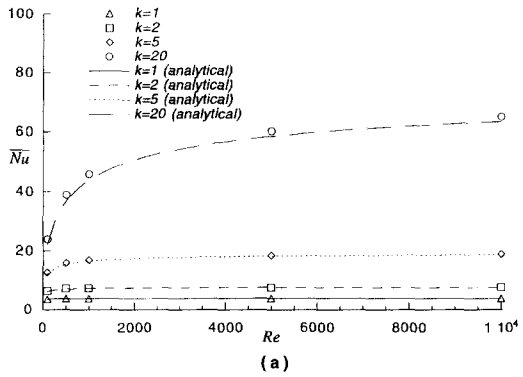

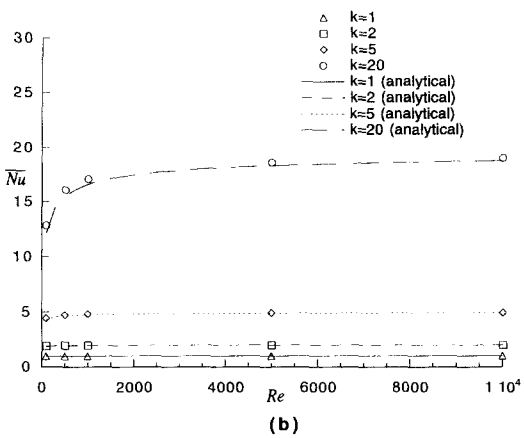

Fig. 13. Average Nusselt number ($\bar{N}u$) vs Re for $Pr = 10^{2}$: (a) $\lambda = 0.25$; (b) $\lambda = 1$.

REFERENCES

1. Heggs, P. J., Ingham, D. B. and Keen, D. J., The effects of heat conduction in the wall on the development of recirculating combined convection flows in vertical tubes. *International Journal of Heat and Mass Transfer*, 1990, **33,** 517–528.
2. Anand, N. K. and Tree, D. R., Some studies of the effects of axial conduction in a tube wall on the steady-state laminar convective heat transfer. *Journal of Heat Transfer*, 1987, **109,** 1025–1028.
3. Bejan, A. and Rossie, A. N., Natural convection in a horizontal duct connecting two fluid reservoirs. *Journal of Heat Transfer*, 1981, **103,** 108–113.
4. Bejan, A. and Kimura, S., Penetration of free convection into a lateral cavity. *Journal of Fluid Mechanics*, 1981, **103,** 465–478.
5. Zebib, A. and Wo, Y. K., A two-dimensional conjugate heat transfer model for forced air cooling of an electronic device. *ASME Journal of Electronic Packaging*, 1989, **111,** 41–45.
6. Nigen, J. S. and Amon, C. H., Time-dependent conjugate heat transfer characteristics of self-sustained oscillatory flows in a grooved channel. *Journal of Fluids Engineering*, 1994, **116,** 499–507.
7. Perelman, T. L., On conjugated problems of heat transfer. *International Journal of Heat and Mass Transfer*, 1961, **3,** 293–303.
8. Luikov, A. V., Aleksashenko, V. A. and Aleksashenko, A. A., Analytical methods of solution of conjugated problems in convective heat transfer. *International Journal of Heat and Mass Transfer*, 1971, **14,** 1046–1056.
9. Luikov, A. V., Conjugate convective heat transfer problems. *International Journal of Heat and Mass Transfer*, 1974, **17,** 257–265.
10. Sakakibara, M., Mori, S. and Tanimoto, A., Effect of wall conduction on convective heat transfer with laminar boundary layer. *Heat Transfer—Japanese Research*, 1973, **2,** 94–103.
11. Payvar, P., Convective heat transfer to laminar flow over a plate of a finite thickness. *International Journal of Heat and Mass Transfer*, 1977, **20,** 431–433.
12. Karvinen, R., Note on conjugated heat transfer in a flat plate. *Letters of Heat and Mass Transfer*, 1978, **5,** 197–202.
13. Karvinen, R., Some new results for conjugated heat transfer in a flat plate. *International Journal of Heat and Mass Transfer*, 1978, **21,** 1261–1264.
14. Chida, K. and Katto, Y., Study on conjugate heat transfer by vectorial dimensional analysis. *International Journal of Heat and Mass Transfer*, 1976, **19,** 453–460.
15. Gosse, J., Analyse simplifiée du couplage conduction–convection pour une écoulement à couche limite laminaire sur une plaque plane. *Revue Générale Thermique*, 1980, **228,** 967–971.
16. Mori, S., Nakagawa, H., Tanimoto, A. and Sakakibara, M., Heat and mass transfer with a boundary layer flow past a plate of finite thickness. *International Journal of Heat and Mass Transfer*, 1991, **34,** 2899–2909.

17. Pozzi, A. and Lupo, M., The coupling of conduction with forced convection over a flat plate. *International Journal of Heat and Mass Transfer*, 1989, **32,** 1207–1214.
18. Yu, W.-S., Lin H.-T. and Hwang, T.-Y., Conjugate heat transfer of conduction and forced convection along wedges and a rotating cone. *International Journal of Heat and Mass Transfer*, 1991, **34,** 2497–2507.
19. Pop, I. and Ingham, D. B., A note on conjugate forced convection boundary layer flow past a flat plate. *International Journal of Heat and Mass Transfer*, 1993, **36,** 3873–3876.
20. Pozzi, A., Bassano, E. and de Socio, L., Coupling of conduction and forced convection past an impulsively started finite flat plate. *International Journal of Heat and Mass Transfer*, 1993, **36,** 1799–1806.
21. Carslaw, H. S. and Jaeger, J. C., *Conduction of Heat in Solids*, 2nd edn. Clarendon Press, Oxford, 1959.
22. Vynnycky, M. and Kimura, S., Conjugate free convection due to a heated vertical plate. *International Journal of Heat and Mass Transfer*, 1996, **39,** 1067–1080.
23. Cebeci, T. and Bradshaw, P., *Physical and Computational Aspects of Convective Heat Transfer*. Springer, Berlin, 1984.
24. Pohlhausen, E., Der Warmeaustausch zwischen festen Korpern und Flussigkeiten mit kleiner Reibung und kleiner Warmeleitung. *Zeitschrift Angewandt Mathematik Mechanik*, 1921, **1,** 115–121.
25. Vynnycky, M. and Kimura, S., Conjugate free convection due to a vertical plate in a porous medium. *International Journal of Heat and Mass Transfer*, 1994, **37,** 229–236.
26. Patankar, S. V., *Numerical Heat Transfer and Fluid Flow*. Hemisphere, Washington D.C., 1980.
27. Robertson, G. E., Seinfeld, J. H. and Leal, L .G., Combined forced and free convection flow past a horizontal flat plate. *AIChE Journal*, 1973, **19,** 998–1008.